



Stochastic modeling of the Earth's magnetic field: Inversion for covariances over the observatory era

N. Gillet

*ISTerre, Université Grenoble 1, CNRS, Grenoble CEDEX 9, France
(nicolas.gillet@obs.ujf-grenoble.fr)*

D. Jault

ISTerre, Université Grenoble 1, CNRS, Grenoble CEDEX 9, France

Earth and Planetary Magnetism Group, Institut für Geophysik, ETH Zürich, Switzerland

C. C. Finlay

Earth and Planetary Magnetism Group, Institut für Geophysik, ETH Zürich, Switzerland

DTU Space, Technical University of Denmark, DK-2800, Kongens Lyngby, Denmark

N. Olsen

DTU Space, Technical University of Denmark, DK-2800, Kongens Lyngby, Denmark

[1] Inferring the core dynamics responsible for the observed geomagnetic secular variation requires knowledge of the magnetic field at the core-mantle boundary together with its associated model covariances. However, most currently available field models have been built using regularization conditions, which force the expansions in the spatial and time domains to converge but also hinder the calculation of reliable second-order statistics. To tackle this issue, we propose a stochastic approach that integrates, through time covariance functions, some prior information on the time evolution of the geomagnetic field. We consider the time series of spherical harmonic coefficients as realizations of a continuous and differentiable stochastic process. Our specific choice of process, such that it is not twice differentiable, mainly relies on two properties of magnetic observatory records (time spectra, existence of geomagnetic jerks). In addition, the required characteristic times for the low degree coefficients are obtained from available models of the magnetic field and its secular variation based on satellite data. We construct the new family *COV-OBS* of field models spanning the observatory and satellite era of 1840–2010. These models include the external dipole and permit sharper time changes of the internal field compared to previous regularized reconstructions. The a posteriori covariance matrix displays correlations in both space and time, which should be accounted for through the secular variation error model in core flow inversions and geomagnetic data assimilation studies.

Components: 13,800 words, 10 figures, 1 table.

Keywords: geomagnetic secular variation; covariances; stochastic processes.

Received 20 July 2012; **Revised** 5 December 2012; **Accepted** 23 July 2012; **Published** 3 April 2013.

Gillet N., D. Jault, C. C. Finlay, and N. Olsen (2013), Stochastic modeling of the Earth's magnetic field: Inversion for covariances over the observatory era, *Geochem. Geophys. Geosyst.*, 14, 766–786, doi:10.1002/ggge.20041.

1. Introduction

[2] Models of the Earth's magnetic field at the core surface are the main agent through which geomagnetic observations are used to infer core dynamics. In this case, knowledge of the second-order statistics (covariances) of the field model coefficients is a prerequisite for attempts to constrain the Earth's core dynamics [Fournier *et al.*, 2011]. The uneven geographical distribution of magnetic observatories and the time-variable accuracy of magnetic measurements give yet more importance to a reliable covariance information for the epochs anterior to the advent, in 1999, of continuous, global satellite coverage. Unfortunately, the regularization conditions that have been introduced to ensure convergence in the presently available core field models are so strong that they lead to unrealistic covariances. For example, spatial regularization has commonly been applied based on a norm measuring the Ohmic heating within the core [Gubbins and Bloxham, 1985], but observations of the heat flux out of Earth's surface place only weak bounds on this quantity [Jackson and Livermore, 2009]. In this case, the comparatively large regularization parameters adopted by most workers (essentially to smooth their models in a visually appealing manner) cannot be rigorously justified [Backus, 1988]. In the absence of trustworthy covariance information, field models with null [Kuang *et al.*, 2009] or "estimated" [Beggan and Whaler, 2009] errors had to be used in the first attempts at Kalman filtering in geomagnetism. The paucity of covariance information is all the more unfortunate given that the small size of geomagnetic models, compared to the size of meteorological and oceanographic models, makes it conceivable to use the full covariance information in geomagnetic data assimilation schemes.

[3] This state of affairs is well illustrated by the simple problem of estimating core surface motions \mathbf{u} through the inversion of the radial induction equation at the core surface [Holme, 2007],

$$\frac{\partial B_r}{\partial t} = -\nabla_{\dot{H}}(\mathbf{u}B_r) + \frac{\eta}{r}\nabla^2(rB_r), \quad (1)$$

where B_r is the radial magnetic field at the core-mantle boundary, η is the Earth's core magnetic diffusivity, and $\nabla_{\dot{H}}$ is the horizontal divergence operator. The lack of reliable covariance information has made it difficult to generalize the ensemble method developed by Gillet *et al.* [2009] for the satellite era (from 1999 onwards) to the observatory era that began in 1840. Eymin and Hulot [2005] and then [Pais and Jault, 2008] identified the

ignorance of the small scale magnetic field (spherical harmonic degree $n \geq 14$) at the surface of the core as the main limitation in the estimation of core surface flows from satellite data. This effect is accounted for through modeling errors on the secular variation (SV) $\partial B_r / \partial t$. Gillet *et al.* [2009] subsequently produced an ensemble of stochastic, time-correlated, small-scale magnetic field models (extrapolated from the statistical properties measured at large length scale) in order to supplement the resolved large-scale field. From this ensemble of magnetic fields, they calculated an ensemble of core flows, all able to explain the observed magnetic field variation.

[4] Generalizing this approach to the observatory era, which amounts to generating an ensemble of field models from the estimated mean and covariances of all the model coefficients (instead of coefficients with degree $n \geq 14$ only), seems to be the appropriate way to account for the lower precision of geomagnetic data at earlier times and for the uneven geographical distribution of geomagnetic surface data. We refer to this approach of using an ensemble of field models, each generated by a stochastic process, to represent the knowledge contained in geomagnetic observations as "stochastic field modeling". This terminology was previously introduced by Gubbins [1983] in the context of building snapshot field models (even though he was effectively using a regularization procedure). In our study, stochastic information is instead used to characterize the variance and temporal autocorrelation function of time-dependent Gauss coefficients. An adequate description of their covariances is a fundamental ingredient since, as noted by Pais and Jault [2008], it is the level of confidence in the main field (MF, or internal field up to degree $n = 14$) coefficients that governs the amplitude of modeling errors, through the amount of unresolved magnetic and velocity fields entering the nonlinear term in (1). As a consequence, the larger the uncertainty in the MF, the larger the SV modeling errors.

[5] Considering the time sequences of magnetic field coefficients as realizations of differentiable continuous time processes φ naturally allows the calculation of the secular variation $\partial B_r / \partial t$, which enters the equation (1). This assumption is consistent with the encouraging agreement between the SV in recent satellite-era field models up to at least degree $n = 10$ [Lesur *et al.*, 2010; Olsen *et al.*, 2010; Finlay *et al.*, 2012]. The large-scale part of the instantaneous SV can be reasonably constrained from satellite data, and we can estimate characteristic times for the spherical harmonic degrees 1 to 10 of the geomagnetic field [Hulot and Le Mouél, 1994]. We use these times as a first constraint on the processes φ . Holme

et al. [2011] and *Christensen et al.* [2012] have recently advocated, using models for the secular acceleration (SA) $\partial^2 B_r / \partial t^2$ of the magnetic field, to estimate an additional timescale, this one for the spherical harmonic coefficients of the secular variation. However, SA estimates are known to depend on the regularization conditions [e.g., *Finlay et al.*, 2012], which indicates that the instantaneous SA, in contrast to the instantaneous SV, is not well defined given the available observations. In this paper, we provide further evidence that only integrals of the SA over finite time intervals can be estimated at present. We therefore choose not to use SA models to constrain the continuous time processes φ sampled by the time series of geomagnetic coefficients. Instead, we construct the required time correlation information from the spectrum of observatory records.

[6] The processes φ are, in an ideal scenario, capable of reproducing the actual physical process governing the time evolution of the magnetic field in only a finite range of frequencies. That range is limited by the time resolution of the internal field that can be extracted from magnetic measurements, (approximately 1 year for the largest length scales [see, e.g., *Olsen and Manda, 2007*]). Such processes φ can be defined by a finite number of parameters, and they need not have the same differentiability properties as the natural processes.

[7] Theoretically, the filtering of magnetic signals coming from the core as they pass through the electrically conducting mantle may also provide us with information concerning the correlation properties of the geomagnetic coefficients series at the Earth's surface. It can be shown that if the mantle electrical conductivity depends only on the radius, the mantle acts as a filter for each spherical harmonic component of the geomagnetic field, with a smoothing time that decreases with degree [*Backus, 1983; Pinheiro and Jackson, 2008*]. This smoothing time can be calculated as a function of a weighted integral of the conductivity. Recent investigations concerning the electrical properties of the mantle from satellite data point to rather low values for the electrical conductivity, of the order of 2 S m^{-1} in the lower mantle [*Kuvshinov and Olsen, 2006; Velínský, 2010*], which correspond to smoothing times of at most a few months. If these estimates are correct, we can treat the mantle as transparent to core signals with annual periods and longer that are considered in this paper.

[8] In section 2, we describe our algorithm for producing an ensemble of magnetic field models for the era 1840–2010. These models account for the geomagnetic observations and possess statistical

properties (including time correlations) that can be encapsulated in a covariance matrix. We define the prior covariance information from the assumption that the Gauss coefficients result from a stationary process. We find that the process obeying a particular second-order stochastic differential equation possesses the required properties. This also leads us to question whether or not one should calculate the instantaneous SA. In section 3, we present our new family of field models, named *COV-OBS*, which include the necessary covariance information, and compare them with previous models, briefly analyzing the series we obtain for the external dipole. In section 4, we discuss perspectives for geomagnetic field modeling, and possible adaptations of our method to less frequently sampled paleomagnetic observations.

2. Stochastic Magnetic Field Modeling Using a Prior Probability Distribution for the Geomagnetic Potential Gauss Coefficients

[9] The conventional method to calculate time-dependent geomagnetic field models involves minimizing the spatial and temporal complexity of the magnetic field at the core surface [*Jackson and Finlay, 2007*]. It ensures that the spatial and temporal power spectra converge toward zero for decreasing length scales and periods, but it does not give a correct representation of the error statistics [*Backus, 1988*]. We adopt instead a Bayesian approach and specify a (Gaussian) prior probability distribution for the geomagnetic potential coefficients [*Gubbins and Bloxham, 1985; Backus, 1988; McLeod, 1996*]. This involves the a priori mean values of the coefficients (all chosen to be zero) and the a priori covariance matrix of model coefficients.

[10] In section 2.1, we describe the geomagnetic data used in our inverse problem. We then discuss the equations relating the Gauss coefficients to the observations (section 2.2), before giving the general methodology to build our ensemble of field models (section 2.3). In section 2.4, we present the information about the time sequences of geomagnetic coefficients that we introduce prior to the calculation of models. Secular variation time-scales calculated using the SA from magnetic field models of the satellite era are not part of this information since we conclude (section 2.5) that these can be strongly influenced by modeling choices and may not be characteristic of the true core field.

2.1. Geomagnetic Data

[11] The observations used in this study are direct measurements of the geomagnetic field spanning the interval from 1840.0 to 2010.0. Except for the most recent decades, it consists of the dataset used by *Jackson et al.* [2000] to produce the *gufm1* field model. During this interval, measurements of absolute intensity are available and data sources include maritime, survey, ground observatory, and satellite observations. Here we provide only a brief overview of the main features of each data set. Statistics summarizing the observations used are found in Table 1.

[12] The land survey and maritime observations used are those compiled by *Jackson et al.* [2000] and *Jonkers et al.* [2003]. Error estimates for these historical records were also allocated using the scheme developed by these authors. Annual means from ground observatories provide the most important source of information regarding the secular variation over the time span of our model. We use first differences of observatory annual means provided by the World Data Center for Geomagnetism (Edinburgh) spanning the period 1840.0 to 2010.0 and comprising all observatories operating during this interval. These data have been manually processed to remove gross outliers and to split observatories where unresolved base line jumps occur. Since we are constructing a model spanning the past 170 years, information is not always available on the manner in which the annual means were computed, and consequently, we do not filter according to the computation method (e.g., all days, quiet days, incomplete, absolute only, etc., cf. *oamformat.doc* file available from BGS). Our annual mean data therefore contains contributions not only from the core but also from large-scale magnetospheric currents, ionospheric currents including the S_q system, and their induced counterparts [*Gavoret et al.*, 1986; *Yukatake and Cain*, 1987;

Schmucker, 1991]. Error estimates were determined for each component at each observatory from the scatter about independent one dimensional penalized spline fits, with a regularization parameter determined by generalized cross validation [*Bloxham and Jackson*, 1992]. We recognize that this method is not fully satisfactory: we assign a single error estimate for time series, whereas the accuracy of magnetic measurements has improved with time. Note that taking the difference between annual means introduces correlation between the secular variation estimates [*Haines*, 1993] that we have not taken into account here. These observatory series and the error estimation scheme are extensions of the approach used in the construction of the *ufm1* [*Bloxham and Jackson*, 1992] and *gufm1* [*Jackson et al.*, 2000] field models.

[13] We also employ satellite data that provide a strong constraint on the field morphology at recent times. We use intensity observations from the POGO series of satellites (1965–1971) [e.g., *Cain and Sweeney*, 1973] and the DE-2 satellite (1981–1983) [e.g., *Langel et al.*, 1988], as well as both intensity and three component vector observations from the Magsat (1980) [*Langel and Estes*, 1985], Ørsted (since 1999) [*Neubert et al.*, 2001], and CHAMP (2000–2010) [*Reigber et al.*, 2002] satellites. The DE-2 data set is that previously employed by *Jackson et al.* [2000]. Since we had access to the original data for the other missions, we decided to re-perform the processing and data selection in a consistent manner, with the aim of producing data sets suitable for co-estimating slow variations in both the core field and the largest scale, quiet-time, external field. As far as possible, we employed the quiet-time selection criteria used in the CHAOS model series [*Olsen et al.*, 2006]. This involves the magnitude of the time derivative of the *Dst* index being less than or equal to

Table 1. Summary of the Statistics for the Various Datasets

Name	Period	X	Y	Z	H	F	I	D	Bias	Misfit
OAM's ^a	1840–2010	12261	12141	11944	–	–	–	–	–0.004	0.936
DE-2	1981–1983	–	–	–	–	451	–	–	–0.239	1.031
POGO	1965–1970	–	–	–	–	7546	–	–	0.009	0.828
Magsat	1979–1980	2273	2286	2290	–	279	–	–	–0.157	0.821
CHAOS-4 ^b	1999–2010	24,619	24,619	24,619	–	3392	–	–	–0.044	1.024
PNAL ^c	1840–1867	–	–	–	–	–	–	13,852	0.036	1.414
Surveys	1840–1980	–	–	10,290	56,381	27,109	41,686	88,209	–0.012	0.872

X , Y , and Z stands for the three Cartesian components of the magnetic field; H , F , I , and D stand, respectively, for horizontal intensity, total intensity, inclination, and declination. The total number of data of is 366,236 with a global normalized misfit of 0.937.

^aOAMs stands for first differences of observatory annual means.

^bCHAOS-4 vector data are rotated in the $\{B_y, B_x, B_z\}$ frame to deal with anisotropic attitude errors [*Holme and Bloxham*, 1996].

^cPNAL stands for Paris national archives and library.

2.0 nT/h and the Kp index being less than or equal to 2°. Vector data were only used below 60° geomagnetic latitude. In addition, Ørsted and CHAMP vector data are only used for times when the sun was more than 10° below the horizon (plus additional selection criteria for CHAMP) [see *Olsen et al.*, 2006], while for Magsat, we selected only dawn data.

[14] Sub-sampling of the original datasets was carried out using a grid of 72 cells in longitude by 36 cells in cosine of co-latitude, refilled each year with random sampling from cells where more than one observation is available, in order to obtain a coverage in space and time as homogeneous as possible. This coverage is sufficiently dense for our purposes because we do not attempt to estimate the crustal field, and because we are interested only in slow field variations with timescales of years and longer. Vector data are selected where possible, with CHAMP data preferred during the most recent decade. We also apply a correction to account for the known part of the crustal field—we take this to be the internal field from the CHAOS-4 model for spherical harmonic degrees 16 to 80. On the other hand, no a priori correction for the external field is applied, enabling satellite data to be used to constrain both the core field and the large-scale external field.

[15] The allocation of a prior error budgets to satellite data is unfortunately very difficult due to the non-stationary, non-Gaussian nature of the unmodeled noise sources. In the present study, it is further complicated because we only solve for the slow variation of the external dipole and do not account for most of the rapidly changing external field, as is the case for most recent satellite field models. Hence, our error estimates are somewhat larger than those discussed for example in the CHAOS and GRIMM series of models. In all cases, we used an error budget varying with geomagnetic latitude taking its maximum value within 25° of the geomagnetic pole and its minimum value within 45° of the geomagnetic equator, with a cosine taper for the intervening 20°. For POGO (respectively Magsat) scalar data, error estimates ranged between 10 and 15 nT (respectively 8 and 18 nT). For Magsat northward, eastward, and downward vector components, the range is 11 to 18 nT, 9 to 19 nT, and 9 to 15 nT, respectively. For Ørsted (respectively CHAMP), error estimates for the scalar data and the isotropic component of the vector data were allocated in the range 5.5 to 8.5 nT (respectively 4 to 10 nT). The pointing error budget does not vary with latitude and is implemented as described in *Finlay et al.* [2012].

2.2. Forward Modeling of the Geomagnetic (Potential) Field

[16] We separate between internal and external field contributions: $\mathbf{B} = \mathbf{B}_i + \mathbf{B}_e$. Both sources are described via potentials: $\mathbf{B}_{i,e} = -\nabla V_{i,e}$. The potential

$$V_i(r, \theta, \phi) = a \sum_{n=1}^{N_i} \left(\frac{a}{r}\right)^{n+1} \sum_{m=0}^n [g_n^m \cos m \phi + h_n^m \sin m \phi] P_{nm}(\cos \theta) \quad (2)$$

accounts for the internal field, where $a = 6371.2$ km is the reference spherical radius of Earth's surface and P_{nm} are associated Legendre functions of degree n and order m . Only coefficients of the internal field $\{g_n^m, h_n^m\}$ with degrees $n \leq N_i = 14$ enter our inverse problem. Coefficients of higher degrees, which also contribute to the magnetic model that will eventually be used to constrain the core dynamics, are controlled entirely by our prior knowledge (see sections 2.3 and 2.4).

[17] The potential V_e is designed to account primarily for time changes of the large-scale external field but also includes the associated secondary field induced in the core, assuming an electrically insulating mantle:

$$V_e(r, \theta, \phi) = a \sum_{n=1}^{N_e} \left(\frac{r}{a}\right)^n \left[1 + \frac{n}{n+1} \left(\frac{a}{r}\right)^{2n+1} \right] \sum_{m=0}^n [q_n^m \cos m \phi + s_n^m \sin m \phi] P_{nm}(\cos \theta). \quad (3)$$

It is restricted to the dipole component (i.e., $N_e = 1$) that we suppose is aligned with the internal dipole field. In geomagnetic coordinates, this can be written as

$$[q_1^0, q_1^1, s_1^1] = \frac{\tilde{q}_1^0}{\sqrt{g_1^{02} + g_1^{12} + h_1^{12}}} [g_1^0, g_1^1, h_1^1]. \quad (4)$$

Given the internal field, the external field is then represented by a single unknown scalar \tilde{q}_1^0 . We performed tests with a more complex external field with $N_e = 3$ and found this does not significantly change the results obtained by assuming $N_e = 1$. Note that we do not account for the nonlinearity that appears in equation (4): at each iteration, the direction of the geomagnetic coordinate system is considered a priori.

[18] At inter-annual periods, electrical currents induced in the core by the large length-scale external field contribute to the observed magnetic field [Velínský and Finlay, 2011]. Approximating the core as a perfectly conducting sphere, the radial

component of the primary external field is canceled at the core-mantle boundary (CMB, $r=c=3485.0$ km) by its induced counterpart, which is accounted for in the second term of V_e in equation (3). Note that accounting for this simple-induced field does not introduce any additional unknowns since it is completely determined by \tilde{q}_1^0 .

[19] The field model coefficients $g_n^m(t)$, $h_n^m(t)$, and $\tilde{q}_1^0(t)$ are expanded in time onto a basis of $P=90$ B-splines of order 4, with knots regularly spaced every 2 years over $[t_s, t_e]=[1838, 2012]$ (we add one extra knot at both the start and endpoints in an effort to mitigate edges effects). This results in an unknown vector \mathbf{b} of size $(N_i(N_i+2)+1)P=20,250$. The choice of a 2 year knot spacing is governed by the studied time interval. Only observatory annual means allow one to constrain the SV as far back as 1840. As a consequence, the knot spacing must be larger than 1 year, in order to prevent unconstrained inter-annual field oscillations, which would not be penalized in our scheme as they would not alter the fit to annual differences. The effect of such a value for the knot spacing, formally described in Appendix 5, is discussed in section 2.5, and a possible future strategy to get rid of splines entirely is proposed in section 4.2.

[20] We can write the forward problem in matrix form as

$$\mathbf{d} = \mathbf{H}(\mathbf{b}) + \mathbf{e}, \quad (5)$$

where \mathbf{d} is the data vector and \mathbf{e} the data error vector, whose statistical properties are characterized by the covariance matrix $C_e = E(\mathbf{e}\mathbf{e}^T)$. The vector \mathbf{b} contains the coefficients for the magnetic field model; it is characterized by an estimate of the a priori mean $\bar{\mathbf{b}}$ (or background, in practice taken to be zero for all internal coefficients) and an a priori covariance matrix $C_b = E(\mathbf{b}\mathbf{b}^T)$ describing the expected perturbation about the background. Our specification of the a priori covariances is described in section 2.4, but it is worth emphasizing here that our a priori covariance matrix is no longer of banded form (as was the case in earlier studies using splines and involving the simple regularization of time derivatives). \mathbf{H} is the forward operator describing the internal, external, and induced signals on inter-annual and longer periods according to the model above.

2.3. Bayesian Solution of the Inverse Problem and Production of an Ensemble From the A Posteriori Covariance Matrix

[21] The Bayesian estimate for the solution to the forward problem (5) with maximum posterior

probability, given the observations and the information on the random variables \mathbf{e} and \mathbf{b} carried by C_e and C_b , is found by minimizing the following cost function [see, e.g., *Sivia and Skilling, 2006*]

$$\mathcal{J}(\mathbf{b}) = [\mathbf{d} - \mathbf{H}(\mathbf{b})]^T C_e^{-1} [\mathbf{d} - \mathbf{H}(\mathbf{b})] + [\mathbf{b} - \bar{\mathbf{b}}]^T C_b^{-1} [\mathbf{b} - \bar{\mathbf{b}}] \quad (6)$$

We estimate the posterior mean model $\bar{\mathbf{b}}$ as the final converged iteration of a Newton-type algorithm,

$$\mathbf{b}_{i+1} = \mathbf{b}_i + C_{i+1} [\nabla \mathbf{H}(\mathbf{b}_i)^T C_e^{-1} (\mathbf{d} - \mathbf{H}(\mathbf{b}_i)) - C_b^{-1} (\mathbf{b}_i - \bar{\mathbf{b}})] \quad (7)$$

where the a posteriori covariance matrix

$$C_{i+1} = [\nabla \mathbf{H}(\mathbf{b}_i)^T C_e^{-1} \nabla \mathbf{H}(\mathbf{b}_i) + C_b^{-1}]^{-1} \quad (8)$$

involves the inverse of the Hessian matrix and $[\nabla \mathbf{H}]_{kj} = \frac{\partial H_k(\mathbf{b})}{\partial b_j}$. By generating samples from the posterior probability density function, defined by $\bar{\mathbf{b}}$ and the final iteration C of the covariance matrix (8), we can provide a useful ensemble representation of the full Bayesian solution to the inverse problem. This can be efficiently performed via the Cholesky decomposition $C = U^T U$ by the following steps:

- Let $\tilde{\mathbf{b}}$ be a Gaussian random variable vector with zero mean and unit variance;
- Then a model $\mathbf{b} = \bar{\mathbf{b}} + U^T \tilde{\mathbf{b}}$ will satisfy (in a statistical sense) the available geomagnetic data given their specified error estimates;
- When there is no constraint from the observations, the ensemble of field models will have statistics specified by the a priori covariance matrix C_b .

2.4. Stochastic Process A Priori Covariances for the Magnetic Field Model Coefficients

[22] We assume that the Gauss coefficients result from a stationary process, that they have zero mean, that the covariance between different coefficients is zero, and that the auto-covariance sequences for all coefficients with same degree n are identical [*Hulot and Le Mouél, 1994*]. We write

$$C_\varphi(\tau) = E[\varphi(t)\varphi(t+\tau)] = \sigma_\varphi^2 \rho(\tau) \quad (9)$$

the covariance function of a realization $\varphi(t)$ of such a process, with the variance $\sigma_\varphi^2 = C_\varphi(0)$ and the correlation function $\rho(\tau) = C_\varphi(\tau)/C_\varphi(0)$.

[23] The stationarity hypothesis implies that the auto-covariance sequence is positive semi-definite [*Percival and Walden, 1993, p. 37*]. This rules out auto-covariance functions of the form put forward

by *McLeod* [1996]—see his equation (17a) with $B_n < 0$. On the other hand, we show in Appendix B that the often-used squared-exponential covariance function [*Hongre et al.*, 1998; *Bouligand et al.*, 2005] corresponds to time series much smoother than the actual time series of geomagnetic field coefficients. More flexible is the family of the Matérn correlation functions [e.g., *Stein*, 1999; *Rasmussen and Williams*, 2006] that are defined as

$$\rho(\tau) = \frac{2^{1-\nu}}{\Gamma(\nu)} \left[\sqrt{2\nu} \frac{|\tau|}{\tau_c} \right]^\nu K_\nu \left(\sqrt{2\nu} \frac{|\tau|}{\tau_c} \right), \quad (10)$$

where K_ν is the modified Bessel functions of the second kind with order ν , and τ_c is a typical correlation time that is discussed further below. Such correlation functions for the particular cases $\nu=1/2$ (Laplace function) and $3/2$ (cf. equation (13) below) are displayed in Figure 1, superimposed with the squared-exponential function defined in equation (B2), all functions using the same characteristic time τ_c . The high frequency behavior of the spectral density $S(f)$ for a random process whose correlation function is defined by (10) is independent of τ_c and such that $S(f) \sim |f|^{-2\nu-1}$ as $|f| \gg \tau_c^{-1}$. Matérn correlation functions (10) define processes that are k -times differentiable in the mean-square sense if and only if $k > \nu$. For example, from (B1) and the Taylor expansion of (10) at the origin, we obtain for $\nu > 1$

$$\frac{C_\varphi(0)^2}{C_\varphi(0)^2} = \frac{\nu}{(\nu-1)\tau_c^2}, \quad (11)$$

where the dot superscript denotes differentiation with respect to time. For $\nu \rightarrow \infty$, the Matérn correlation

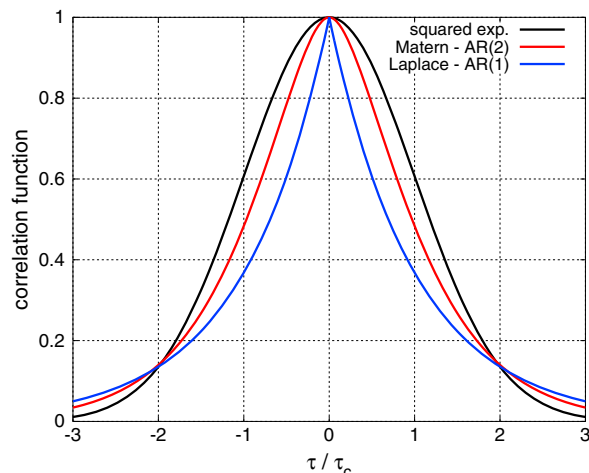


Figure 1. Examples of correlation functions mentioned in this study: squared-exponential in black, Matérn-AR(2) in red, and Matérn-AR(1) (or Laplace) in blue.

function tends to the smooth squared-exponential covariance function defined in equation (B2).

[24] The Matérn correlation functions (10) were first used in turbulence theory because the corresponding spectral density $S(f)$ asymptotically behaves as a power function of the frequency [*Yaglom*, 1987, vol. 1, p. 139 and vol. 2, p. 50]. Indeed, *Von Kármán* [1948] found it appropriate, with $\nu=1/3$, to characterize the correlation of the velocity components observed at two points as a function of their distance, which is a quantity accessible to measurement. The fact that (10), with $\nu=1/3$, defines a random process that is not differentiable was not seen as a problem since the correlation of velocity components measured at an asymptotically close pair of points is not a measurable quantity. Furthermore, this description holds only for particles whose separation is at inertial scales, i.e., greater than the viscous scale. Such a description is thus valid for a finite range of wave numbers.

[25] The special case $\nu=3/2$ corresponds to a continuous time autoregressive (AR) process of order 2 that obeys the stochastic differential equation

$$\frac{d^2\varphi}{dt^2} - \frac{3}{\tau_c^2}\varphi = \varepsilon(t). \quad (12)$$

The white Gaussian random forcing term $\varepsilon(t)$ is a stationary process with zero mean and Dirac autocovariance function. It is thus only in the sense of distributions that realizations of the stochastic processes ε and $d^2\varphi/dt^2$ are defined [see *Jazwinski*, 1970, chap. 3]. Realizations of $d\varphi/dt$ are then continuous but not differentiable. For this special case, the expression (10) can be transformed into

$$\rho(\tau) = \left[1 + \sqrt{3} \frac{|\tau|}{\tau_c} \right] \exp \left(-\sqrt{3} \frac{|\tau|}{\tau_c} \right). \quad (13)$$

Modeling the time evolution of magnetic field coefficients as a stochastic process defined by (12) is attractive as it does not preclude slope changes in the SV, or “jerks”. Also, the asymptotic behavior of its associated spectral density, $S(f) \propto |f|^{-4}$, fits well with the spectrum for the geomagnetic observatory series in the range $5 - 10^2$ years [*Currie*, 1968; *De Santis et al.*, 2003]. Considering that the large length-scale magnetic field can be deduced from ground geomagnetic series, it seems reasonable to construct prior autocorrelation functions for the low spherical harmonic coefficients consistent with the observatory time series. For the sake of parsimony, we consider a similar form of prior to also describe the statistics at higher degrees.

[26] In our a priori covariance function, we thus chose to fix $\nu=3/2$ in the Matérn function (10) and to work with AR(2) stochastic processes. For each coefficient, we must assign a variance σ_g^2 and a correlation time τ_c . These are inferred from the analysis of the MF and SV from the satellite model *gufm-sat-E3* [Finlay et al., 2012], although other satellite models give very similar estimates. For all coefficients of degree n , the a priori variance is defined from the coefficients of the satellite field model estimated in the middle of the satellite decade (to minimize end-effects):

$$\sigma_g^2(n) = \frac{1}{2n+1} \sum_{m=0}^n \left[g_n^m(t)^2 + h_n^m(t)^2 \right]_{t=2005.0}. \quad (14)$$

Using the definition [Hulot and Le Mouél, 1994]

$$\tau_g(n) = \sqrt{\sigma_g^2(n)/\sigma_g^2(n)}, \quad (15)$$

with $\sigma_g^2(n)$ defined as in equation (14), we calculate for all degrees the correlation time $\tau_c(n)$ directly from the expression (11) together with equation (9):

$$\tau_c(n) = \sqrt{3}\tau_g(n). \quad (16)$$

[27] We show in Figure 2 an example of synthetic ground-based SV observatory series obtained from random Gauss coefficients with variances, correlation function, and correlation times given by equations (14), (13), and (16), respectively. A field model satisfying such Matérn-AR(2) prior properties is found to produce SV features visually very similar to those recorded in geomagnetic observatories at inter-annual and decadal timescales. Interestingly, even though the second time derivative is undefined everywhere, major changes in the magnetic field trend do not occur all the time. Such processes also possess a high-frequency content at periods below 1 year (blue curve), which is filtered out when looking at the usual annual differences of monthly values (green curve).

[28] Finally, we must estimate an a priori variance and background for the external coefficient \tilde{q}_1^0 , which is assumed to be uncorrelated with the internal field (excluding that part induced by external variations explicitly described above). To do this, we choose to use an analysis of the past decade when the internal/external separation is more robust, even though it covers only a single solar cycle. A spline fit to the CHAOS-4 [Olsen et al., 2010] quiet-time \tilde{q}_1^0 gives an RMS of about 40 nT^2 and a time average

close to 20 nT. This is in agreement with the findings of Lühr and Maus [2010], who obtained a static component about 8 nT in the Geocentric-Solar-Magnetospheric (GSM) frame plus an additional component of between 2 and 17 nT in the Solar-Magnetic (SM) frame over the period 2000–2010. It also compares well with an independent estimate by Langel and Estes [1985] in 1980 derived from Magsat data. Our external dipole prior is then a 20 nT background plus a 40 nT^2 covariance, with no time correlation (the temporal smoothness of \tilde{q}_1^0 is governed, outside the data, by and the knot spacing and order of the splines).

2.5. On the Significance of Secular Variation Timescales

[29] In this section, we report synthetic tests investigating the ability of recent time-dependent field models covering the satellite era [Olsen et al., 2010; Lesur et al., 2010; Finlay et al., 2012] to describe the temporal regularity of the geomagnetic field. We pay special attention to the use of B-splines and the impact of the temporal regularization. These tests have important implications for recent discussions of the timescales associated with changes in the secular variation [Holme et al., 2011; Christensen et al., 2012].

[30] Historical field models have typically used cubic (i.e., order 4) B-splines as temporal basis functions [Jackson and Finlay, 2007]. Using cubic B-splines to smooth a time series $\varphi(t)$ over an interval $[t_0, t_1]$ leads one to minimize $\int_{t_0}^{t_1} |\partial^2 \varphi / \partial t^2|^2 dt$ [see de Boor, 2001]. But this property was undesirable when workers became interested in $\partial^2 \varphi / \partial t^2$. As a result, the most recent models covering the satellite era incorporate B-splines of order 6 and instead minimize $\int_{t_0}^{t_1} |\partial^3 \varphi / \partial t^3|^2 dt$ (plus an extra constraint on the SA at endpoints). We investigate models of this type in our tests.

[31] The input for the tests was constructed as follows. We generated synthetic time series of internal field coefficients (up to degree 14) over a 10 year period, such that they satisfy the statistical properties of the AR(2) process defined by the equations (13) and (16). All coefficients at a given epoch are uncorrelated (i.e., there is no spatial correlation). These series were then evaluated to create synthetic observations of the vertical Z component of the field at satellite altitude (350 km) in each of 1280 cells of a global spherical triangle tessellation, giving an

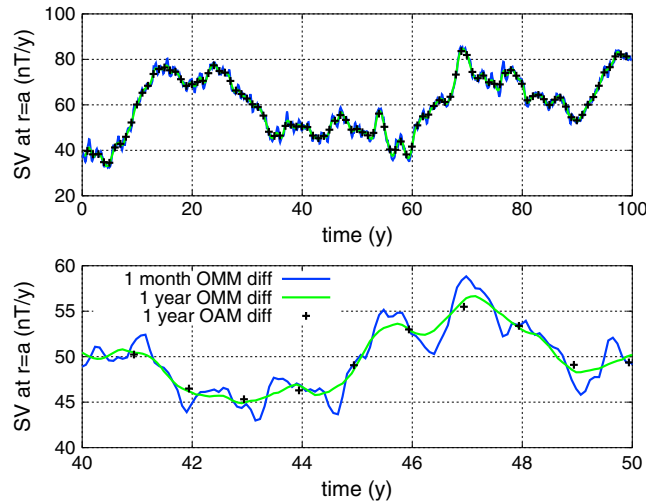


Figure 2. Differentiated observatory series (in nT/year) generated from synthetic spherical harmonic coefficients defined with a Matérn-AR(2) prior (top: over one century; bottom: zoom over one decade): annual differences of annual means (black crosses), annual differences of monthly means (green), and monthly differences of monthly means (blue).

approximately equal area distribution. Synthetic data were generated in each cell every 0.2 years.

[32] Using these (noise-free) observations, we then inverted for an internal field model expanded up to spherical harmonic degree 14 and parameterized in time using sixth-order B-splines. The third time derivative is penalized, and the SA is forced to zero at endpoints, in order to mimic the regularization applied in recent field models. A series of models were constructed using different levels of temporal regularization (i.e., different choices of damping parameter). The influence of the knot spacing was also investigated. For each model setup, we separately inverted 50 synthetic datasets, each constructed to have the same statistics.

[33] Since the B-splines that we use in this test have order larger than 4, the resulting model prediction time series are C^2 continuous. Both their SV and SA spectra are thus well-defined quantities, as is the timescale for changes in the secular variation

$$\tau_{\dot{g}}(n) = \sqrt{\sigma_{\dot{g}}^2(n)/\sigma_g^2(n)}, \quad (17)$$

with $\sigma_{\dot{g}}^2(n)$ defined similarly to equation (14). We find the input value of $\tau_{\dot{g}}$ is well recovered in the field models derived from our synthetic data. This indicates that use of sixth-order B-splines, third time derivative regularization and second time derivative end penalties does not much affect $\tau_{\dot{g}}$, provided this quantity is significantly larger than the knot spacing. On the other hand, the inferred values of $\tau_{\dot{g}}$ are found to depend heavily on the modeling assumptions, in particular on the choice of damping parameter and the knot spacing.

[34] Figure 3a displays the results for the inferred timescales $\tau_{\dot{g}}$, calculated in the middle of the 10 year model time span and averaging over the 50 synthetic input datasets. With no damping, as we increase the knot spacing from 0.5 to 2 years, $\tau_{\dot{g}}$ is shifted toward higher values, though still lower than that found in recent satellite field models. $\tau_{\dot{g}}$ is however found to markedly increase at all degrees as the damping parameter (measuring the weight given to the third time derivative temporal regularization) is increased from zero. As the damping parameter increases, the inferred $\tau_{\dot{g}}$ becomes very large at high degree. This is because penalizing the third time derivative tends to make the SA constant in time and the applied end penalties then force the SA to be small throughout, especially at high degree, as discussed in *Finlay et al.* [2012]. This is illustrated in Figure 3b which presents the spatial power spectra of the SA at the CMB,

$$S_{SA}(n) = (n+1)(2n+1)\left(\frac{a}{c}\right)^{2n+4} \sigma_{\dot{g}}^2(n), \quad (18)$$

calculated in the middle of the 10 years time span. In practice, the temporal damping parameter is often chosen in order to control unphysical model oscillations associated with unmodeled external fields and undesirable variations in the data distribution; these ingredients are absent in our synthetic tests; hence, we are able to construct models with no applied regularization and quantify the impact of gradually increasing the damping parameter on $\tau_{\dot{g}}$.

[35] The SA power for our unregularized synthetic models (Figure 3b) is significantly higher than that possessed by recent satellite-era field models.

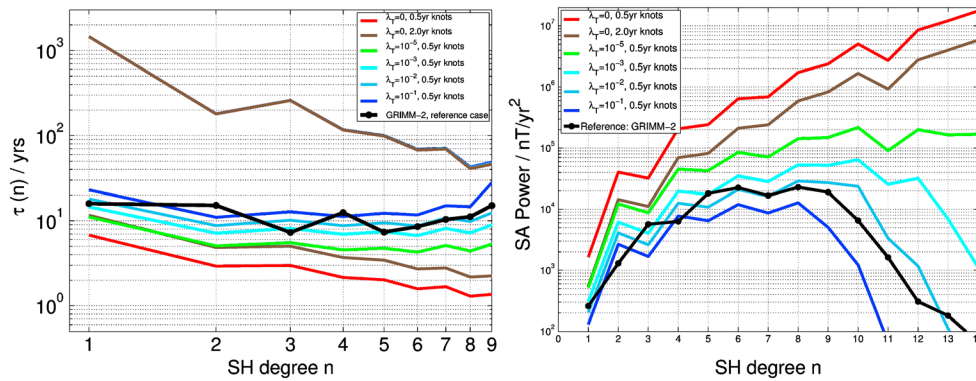


Figure 3. Left panel: timescales τ_g (top curves, all being almost superimposed) and $\tau_{\dot{g}}$ (bottom curves) as a function of the spherical harmonic degree n , as defined in equations (15) and (17). Right panel: SA spatial power spectra as defined in equation (18), for field models projected onto splines with various knot spacing Δt , and calculated for various damping parameters λ_T from synthetic data obtained from random AR(2) spherical harmonic coefficients series. On both plots, the values for the GRIMM-2 model in 2005 are shown for reference (black line with circles).

However, most of this large SA power resides at high frequencies that cannot be captured by such models due to the strong temporal regularization applied to handle the high frequency, unmodeled signals of external origin. The input power at high frequency in the AR(2) series is strongly filtered by taking annual differences of monthly means. Then SV changes very similar to that usually observed are obtained—see the example time series presented in Figure 2. One conclusion from these tests is that existing satellite-era field models, with their implicit temporal regularization and knot spacing, do not actually capture the instantaneous SA. Rather they report a weighted time-integrated SA (which is a well-defined property of an AR(2) process) but with the weighting kernel varying both with spherical harmonic degree and with the chosen damping parameter.

[36] To summarize, these tests suggest that recently inferred values for $\tau_{\dot{g}}$ of approximately 10 years may be affected by the filtering inherent in the regularized spline modeling approach (see Silverman [1984], for a discussion of the relevant smoothing kernels). Regularized, spline-based, field modeling unavoidably produces a filtered picture of the true core state that depends on (i) the continuity properties of the basis functions, (ii) the number of functions employed (here the knot spacing), (iii) possible conditions applied at endpoints, and (iv) the level of temporal regularization applied. Furthermore, if an AR(2) process is an appropriate description (i.e., if a spectral slope of -4 continues to hold for the entire frequency band under consideration), then the instantaneous SA is not a well-defined quantity. As a consequence, we urge caution when quantitatively

interpreting the presently available values for instantaneous $\tau_{\dot{g}}$ directly in terms of core processes [e.g., Holme *et al.*, 2011; Christensen *et al.*, 2012]. In section 4.2, we discuss how these difficulties might be better handled in the future, by adopting a strategy whereby model time dependence is directly controlled by the time correlation statistics of the a priori model, and the B-spline basis is avoided altogether.

3. Results and Discussion of the COV-OBS Family of Geomagnetic Field Models

[37] In this section, we present the main features of our COV-OBS family of magnetic field models. We begin in section 3.1 by presenting evidence for inter-annual changes originating from the core in the secular variation recorded at ground-based observatories. Next, we describe in section 3.2 inter-annual to decadal variations in the external dipole field. Finally, in section 3.3, we present our main result, the a posteriori model error covariance matrix associated with the time series of magnetic field coefficients.

3.1. Evidence for Inter-Annual Secular Variation Changes

[38] We compare in this section COV-OBS and previous geomagnetic field models, all of which are regularized such that small length scales and fast time changes are penalized. The comparison is however restricted by the lack of covariance information for the previous models. A detailed description of the models we compare to (or earlier versions of them)

can be found in *Gillet et al.* [2010]; here we only briefly list their main features:

- *gufm1* [*Jackson et al.*, 2000] is a field model spanning 1590–1990 derived from historical records, observatory annual means, and satellite observations. These include some of the dataset we use here (cf. section 2.1). The data constraint on the SV largely comes from first differences of observatory annual means. The model is regularized at the CMB, in time penalizing second time derivatives, and in space using the Ohmic heating norm.
- CM-4 [*Sabaka et al.*, 2004] is a comprehensive model covering 1960–2002, in which the several sources from the magnetosphere, ionosphere, crust, and core are co-estimated. The second time derivative and the surface Laplacian of the SV are penalized at the CMB.
- C³FM-2 [*Wardinski and Lesur*, 2012] is a field model that has been co-estimated together with a toroidal flow model from first differences of observatory monthly means spanning 1957–2008, using the frozen-flux induction equation as a weak constraint [*Lesur et al.*, 2010]. This process brings in valuable spatial covariances, but it still relies on damping parameters that control the core

surface velocity and the flow acceleration, which indirectly penalize the time evolution (SV and SA) of the magnetic field model.

- GRIMM-2 [*Lesur et al.*, 2010] is a satellite field model covering 2001.0–2009.5, built with alternative data selection criteria compared to that of the CHAOS-4 and *gufm-sat* models and thus distinct from the present study. The third time derivative is penalized at the CMB, and the SA forced to be zero at both endpoints.

[39] In Figure 4, we present the observed SV changes at the Kakioka and Sitka ground magnetic observatories, together with the predictions from our ensemble of field models. Interestingly, an important part of what would sometimes be considered as a scatter in the data is well explained by also including a one parameter external field model. The external field is discussed in more details in section 3.2. Some long-period variations of the external field that we have been unable to recover may have been mapped into variations of the internal field. The remaining misfit between our models and the observatory annual mean data is likely partly due to non-core signal (besides the dipolar external/induced fields), for example, due to S_q current systems that have not been

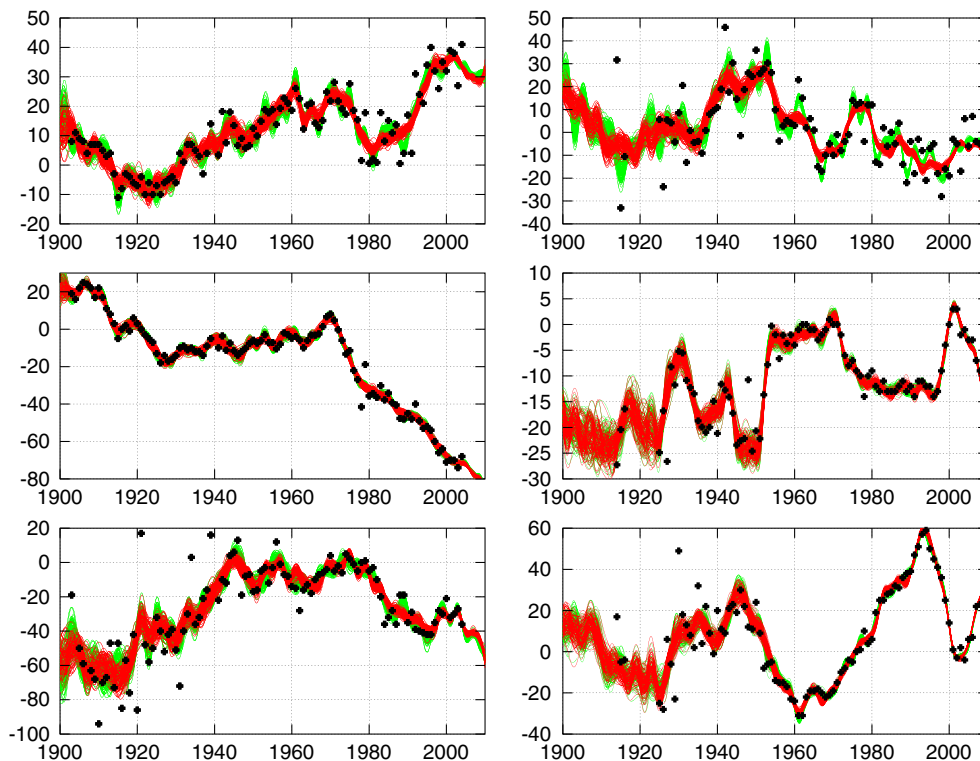


Figure 4. From top to bottom: X, Y, and Z components of the secular variation (in nT/year) for the period 1900–2010, at the Sitka observatory (57N, 136W, left) and at the Kakioka observatory (36N, 140E, right). First differences of observatory annual means (black crosses) are shown compared with predictions from an ensemble of 100 COV-OBS realizations: internal field only (red) and internal plus external fields (green).

averaged out [Gavoret *et al.*, 1986; Yukatake and Cain, 1987; Schmucker, 1991].

[40] The dispersion in the ensemble of predictions increases toward earlier times due to fewer or less reliable data (see all components at Kakioka and especially *Z* at Sitka): the a priori information then controls the statistics of the field models. The dispersion can also differ greatly between components (see *Y* and *Z* at Sitka). All field models nevertheless adequately fit the data in a statistical sense: each is a possible description of the magnetic field variations, given the data uncertainties and the a priori model statistics we have specified. Note that since we used a constant error estimate per observatory series (see section 2.1), the data quality has been under-estimated toward the most recent epochs, for which the dispersion in the ensemble of model predictions and model parameters might thus be over-estimated. In future efforts, it may be worthwhile to account for time-dependent errors for observatory measurements, especially for series starting before 1960 and the use of proton magnetometers. We now leave the world of observations and shift attention to time changes of the Gauss coefficients.

[41] In Figure 5, we compare the evolution of a number of SV coefficients $\partial g_n^m / \partial t$ for our ensemble of field models with the previously published models listed above. As expected, *COV-OBS* realizations display sharper changes in some of the SV coefficients compared to regularized field models, especially at smaller length scales. Indeed, heavily penalizing rapid variations (especially for high degrees) in regularized reconstructions has two consequences. First, the temporal evolution appears too smooth and time sequences of some coefficients lie outside the ensemble range even when data are of relatively good quality—see the comparison with time changes of the *gufm1* model coefficients, for instance, g_{10}^5 around 1975, g_5^5 in 1950 and before 1900, g_2^1 around 1935, 1880, etc. Second, in order to correctly fit the data, regularized models sometimes show more time variability in some low degree coefficients compared to the average *COV-OBS* model. This is observed for the axial dipole trend of *gufm1* before 1930, or that of CM-4 and C³FM-2 around 1980, although in the case of CM-4, this could also be due to the differences in the treatment of the external field and for C³FM-2 to the alternative technique used for allocating data errors [see *Wardinski*

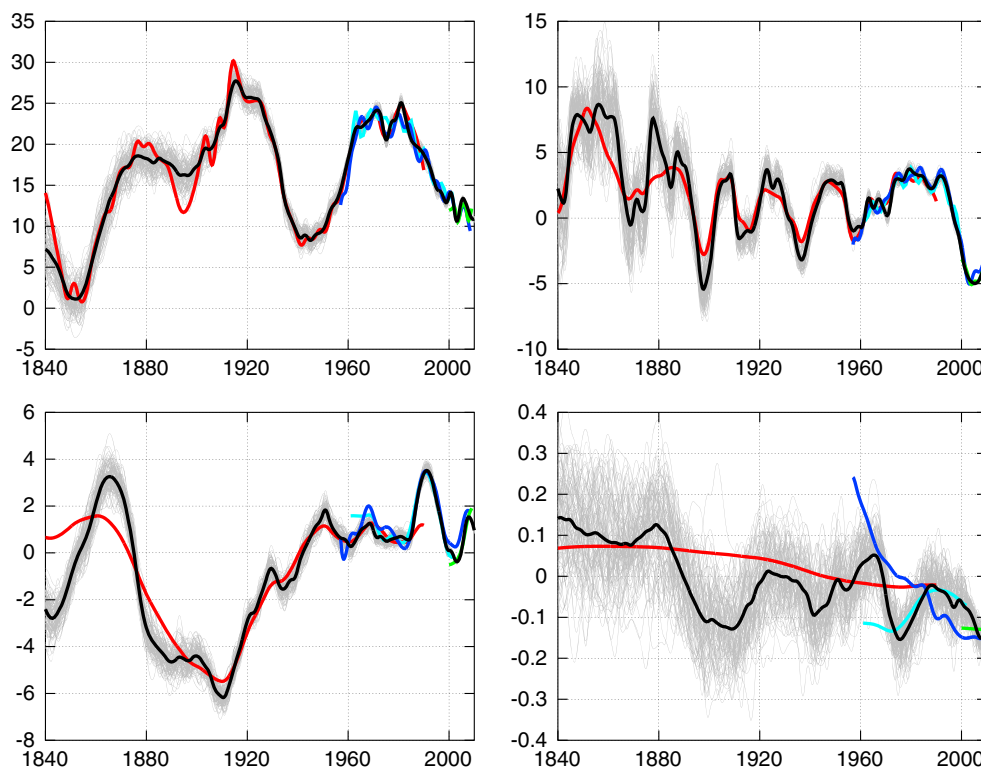


Figure 5. Evolution of SV coefficients $\partial g_n^m / \partial t$ (in nT/yr), for the period 1840–2010, for an ensemble of 100 realizations of the *COV-OBS* field model (gray), the *COV-OBS* mean model (black), *gufm1* (red), C³FM-2 (blue), CM-4 (cyan), and GRIMM-2 (green): $\{n, m\} = \{1, 0\}$ (top left), $\{2, 1\}$ (top right), $\{5, 5\}$ (bottom left), and $\{10, 5\}$ (bottom right).

and Holme, 2011]. The use of different data sets may also explain part of the differences observed between the latter two models and the *COV-OBS* realizations.

[42] In line with the dispersion in model predictions at ground-based observatories, the dispersion of the ensemble of coefficients increases going back in time when the data constraint becomes weaker. Before 1960 and the advent of proton magnetometers, the dispersion in the ensemble of degree 10 spherical harmonic coefficients is much larger than the typical value for the mean model, which means such coefficients are not resolved. For the last 50 years however, the dispersion decreases, and we find that part of the SV changes might be retrieved even at such degrees (see section 3.3). Although the comparison of the *COV-OBS* model with satellite field models at large to moderate length scales is rather good (notwithstanding the different ways of processing the data and different external field models), the SV at degree 10 is certainly much smoother in regularized field models. This may indicate that the SV changes above degree 10 are not adequately resolved in such models.

[43] Given the extra temporal roughness allowed by our stochastic approach, one could be worried

about external field leaking into our internal model. This concern is actually at the origin of the co-estimation of the external dipole. However, we find no evidence (see Figure 5) for non-core signals leaking into our model more than into other models. A regularized model like *gufm1* actually shows oscillations in the axial dipole that we do not require in the *COV-OBS* model. Given the fact those two models are built from very similar datasets, it suggests the extra roughness made possible by our stochastic approach does not lead to more leakage of the external field into the internal field than is the case with classical regularization methods. Also over the interval 2000–2010, the *COV-OBS* model does not display any more fluctuations than other, traditionally regularized, models dedicated to the satellite era, even though we use satellite data that include the external signal. Note that during this period, we consider larger data error estimates than those normally inferred from dedicated satellite field models (see section 2.1), which increases the posterior uncertainty on model coefficients. We emphasize that one should never consider the mean model alone, but use it together with the posterior covariance matrix (or the statistics of the ensemble of models), that

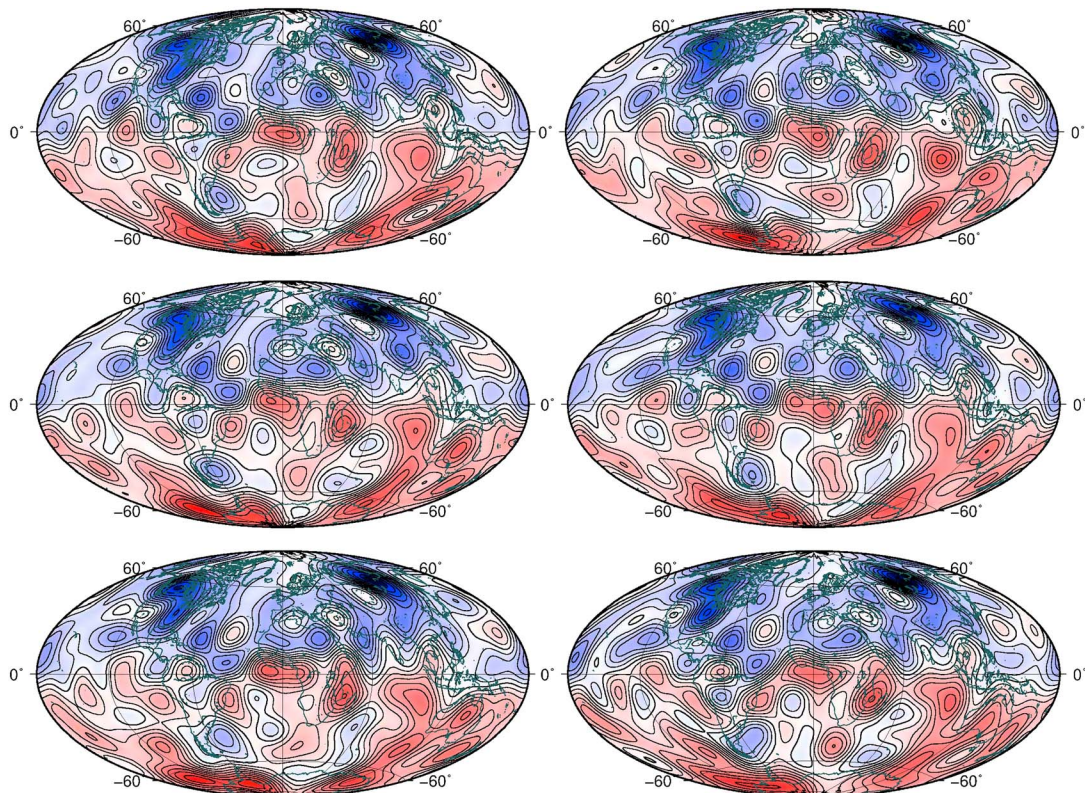


Figure 6. Radial magnetic field B_r at the CMB in 1920, for several realization of the *COV-OBS* model, truncated at $n = 14$. The color scale ranges from -1 mT (dark blue) to $+1$ mT (dark red), with contours every 0.1 mT.

measure how much one should trust the recovered coefficients changes.

[44] In Figure 6, we display maps of the core surface radial field in 1920, for several realizations from our ensemble of field models, all truncated at $n=14$. Each of these maps represents one possible realization of the state of the field (up to degree 14) at that epoch. All show different numbers and shapes of the null-flux curves defined by $B_r=0$. We also present (see Figure 7) the standard deviation of B_r at the core surface in 1920 for the ensemble of models truncated at degrees 10 and 12. It is found that the data constraint is tighter in the northern hemisphere and below the continents. This conclusion, however, holds only for the large-scale magnetic field. There is not such a thing as a pointwise estimate of the uncertainty for the radial magnetic field as the variance of the geomagnetic coefficients strongly increases with the truncation degree (it doubles when changing the truncation from $n=10$ to 12). As a consequence, we conclude that using the $B_r=0$ curves to attest the validity (or not) of the frozen-flux approximation, which has been the focus of numerous papers, is a difficult exercise, even in the ensemble framework we have adopted in this study.

3.2. Inter-annual to Decadal Changes in the Large-Scale External Field

[45] As part of our scheme, we co-estimate time variations of an external axial dipole arranged in dipole coordinates. The result for this component is presented in Figure 8, again using an ensemble of

50 stochastic realizations, shown together with the mean model. Our results agree well with previous estimates of this component of the external field derived using satellite vector data, in particular the 1980.0 estimate of *Langel and Estes* [1985] derived from Magsat data and the estimate from the CHAOS-4 model of *Olsen et al.* [2010] that spans the past decade (the CHAOS-4 output is shown only between 2000 and 2010, considering only quiet times and taking annual means to aid the comparison). Figure 8 also presents comparisons with two previous time-dependent models of the external dipole, on inter-annual and longer timescales, spanning the mid to late twentieth century by *Sabaka et al.* [1997] (partly constrained to be close to the *aa* index, especially before 1940) and by *McLeod* [1996], respectively. Our model contains features from both the previous models. It shows peaks at approximately the same times as the model of *Sabaka et al.* [1997] but without the trend of increasingly maxima between 1920 and 1960. Similar to the model by *McLeod* [1996], we find shorter period variations with lower amplitude between 1960 and 1970.

[46] The dispersion in our ensemble of model realizations decreases markedly toward the present day as the geographical distribution and quality of observations improve. In the earliest part of the model, the variance in the ensemble is comparable with the 40 nT^2 assumed in our a priori variance. Furthermore, it seems we have little sensitivity to the absolute level of $\tilde{q}_1^0(t)$ early in the model, with the mean remaining close to the assumed a priori level of 20 nT. Nonetheless, there is some evidence for coherent decadal

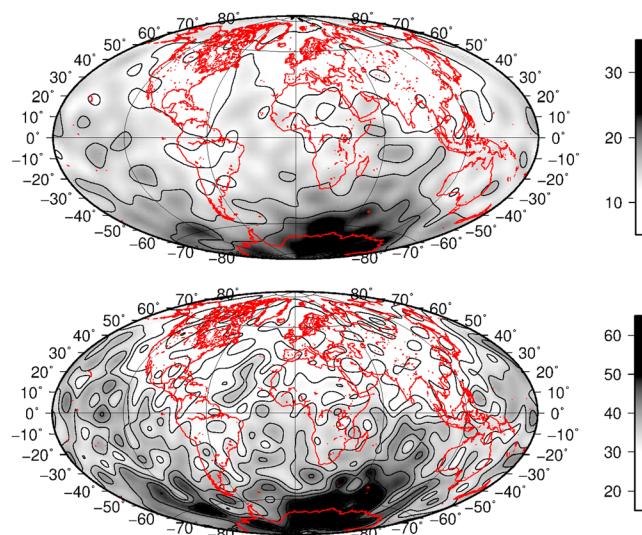


Figure 7. Standard deviation, in an ensemble of 100 *COV-OBS* realizations, of the radial magnetic field at the CMB in 1920, for models truncated at spherical harmonic degree 10 (top) and 12 (bottom)—contours are every 5 nT on both plots, but note the change in scale.

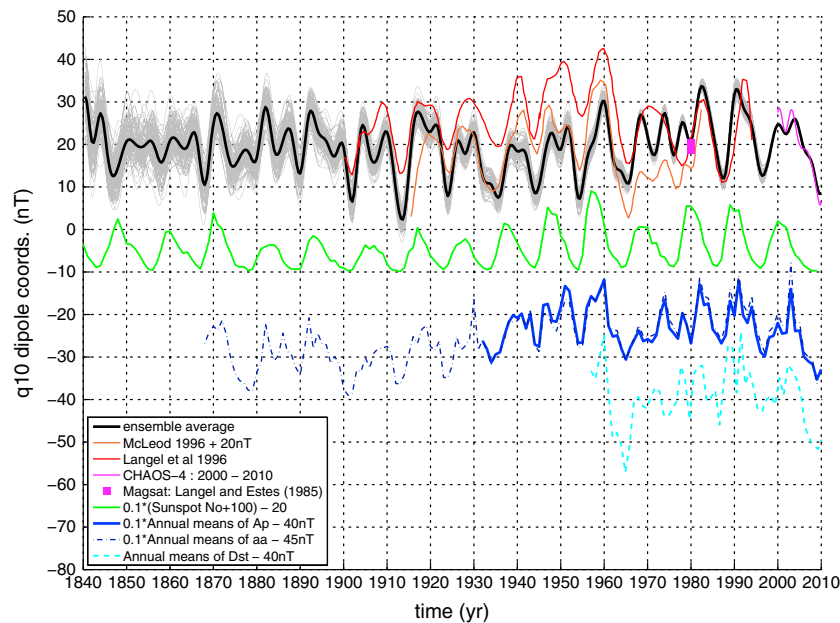


Figure 8. Time series for an ensemble of 100 realizations of the *COV-OBS* external dipole model $\tilde{q}_1^0(t)$ (gray) and the *COV-OBS* ensemble mean (black), together with the models of *Langel et al.* [1996] (red line), *McLeod* [1996] (brown line), *Olsen et al.* [2010] (CHAOS-4, magenta line), and *Langel and Estes* [1985] (Magsat, magenta squares). Also shown (shifted from zero) are annual means of the international sunspot number (green line), the *Ap* index (solid blue line), the *aa* index (dashed blue line), and the *Dst* index (dashed cyan line).

variations in the early part of the model, and modulations in the amplitude of these oscillations may provide information on long term changes in solar activity. Our inability to determine the long-term absolute level of $\tilde{q}_1^0(t)$ means that the internal and external parts of the dipole are unfortunately not completely separated. Analysis of the posterior covariance matrix shows significant correlations between the posterior errors on \tilde{q}_1^0 and that in some internal Gauss coefficients. For instance, we find posterior error correlations up to -0.75 (respectively 0.25) with g_1^0 (respectively h_1^1) at the most recent epoch, when the data error amplitude is the smallest. These correlations gradually decrease toward 1900: as the data constraint becomes weaker, the posterior covariance matrix defined in equation (8) becomes more and more influenced by the prior information, which is empty of correlation between \tilde{q}_1^0 and the internal field coefficients.

[47] The amplitude of the quiet-time external dipole is known to depend on the solar cycle. *Lühr and Maus* [2010] have recently found that the component of the external dipole in GSM coordinates changed little in the most recent solar cycle (amplitude approximately 8.5 nT) while that in SM coordinates varied between 2 nT and 17 nT. This is consistent with the variations between 9 nT and 26 nT that we infer in the past 10 years. Given this dependence on

solar cycle, it is also of interest to compare our results with indicators of both solar and geomagnetic activity. Figure 8 therefore also displays annual means of the international sunspot number, annual means of the *Ap* index (a range index that relies on 13 observatories from mid-latitudes) and annual means of the *aa* index (a longer running range index often showing similar features as *Ap* but relying on just two observatories), and annual means of the *Dst* index.

[48] The *COV-OBS* external dipole model clearly contains the signature of the approximately 11 year variation in solar activity but shows additional peaks that are also evident in the *Ap* and *aa* indices (and to some extent in *Dst*), especially in the declining phase of the solar cycle. The occurrence of two peaks in geomagnetic activity per solar cycle is a well-known phenomenon [*Bartels*, 1963; *Yukatake and Cain*, 1979; *Siebert and Meyer*, 1996]. The first peak is related to the maximum in solar activity, observed when there is a maximum in the amount of magnetic flux generated by the solar dynamo that subsequently emerges through the solar surface giving rise to a maximum in the magnitude of the interplanetary magnetic field. The second peak is thought to be linked to the appearance of recurrent coronal holes in the descending phase of the solar cycle. These cause enhanced solar wind speeds and are associated

with increased geomagnetic sub-storm activity causing enhanced field aligned currents and electrojet activity. The interplay between these different sources may be a reason for the inter-annual variability in observatory monthly means recently noted by *Wardinski and Holme* [2011]. Note that since our model relies on observatory annual means (averaged over all geomagnetic conditions) from all latitudes, our $\tilde{q}_1^0(t)$ series cannot simply be interpreted as an indicator of ring current activity; in particular, like Ap , it is also affected by sub-storm activity.

[49] The main advantages of our approach compared to previous models of long-term variations in the external dipole are (i) that we consistently co-estimate the amplitude of external field variations and secular variation, rather than relying on baselines given by an independent core field model and (ii) that we do not rely on other indices as a constraint, in contrast, for example, to the preferred model of *Sabaka et al.* [1997] that implicitly involved the aa index. Consideration of an ensemble of models, a central aspect of our approach, is also found to be convenient for visualizing the range of possible solutions for the external dipole that are compatible with the observations.

3.3. The Secular Variation Error Covariance Matrix, as Required for Studies of Core Dynamics

[50] In order to use the present results to study the state of the core, it is necessary to concatenate the *COV-OBS* model (mean and covariance) for $n \leq 14$ with a statistical description of the small-scale magnetic field for $n \geq 15$ that cannot presently be directly constrained

by geomagnetic measurements. Using the a priori covariance matrix, as presented in section 2.4, to determine the statistics of $n \geq 15$ coefficients will ensure that the treatment of coefficients with degrees respectively smaller and larger than 14 is consistent.

[51] Models of the SV are used as input “data” when inverting for the core state. We show in Figure 9, for several epochs, the ensemble average of the SV spatial spectra at the CMB (NB: this is different from the spectra of the ensemble average),

$$S_{SV}(n, t) = (n + 1) \left(\frac{a}{c}\right)^{2n+4} \sum_{m=0}^n E \left[\left(\frac{\partial g_n^m}{\partial t} \right)^2 + \left(\frac{\partial h_n^m}{\partial t} \right)^2 \right]. \quad (19)$$

superimposed with the SV spatial spectra for the standard deviation in the ensemble of models

$$S_{\delta SV}(n, t) = (n + 1) \left(\frac{a}{c}\right)^{2n+4} \sum_{m=0}^n E \left[\left(\frac{\partial g_n^m}{\partial t} - \frac{\partial \bar{g}_n^m}{\partial t} \right)^2 + \left(\frac{\partial h_n^m}{\partial t} - \frac{\partial \bar{h}_n^m}{\partial t} \right)^2 \right]. \quad (20)$$

We can see that S_{SV} does not change much throughout the full observatory era: our ensemble of SV models shows rather stationary spectral properties, contrary to previous regularized models [see *Gillet et al.*, 2010]. However, there is a clear decrease of $S_{\delta SV}$ with time, and Figure 9 illustrates how confidence in our SV models increases as observatory data become more numerous and of better consistency, including the advent of scalar proton magnetometers around 1960. The quality gap on the introduction of vector satellite data is also obvious. For instance, we can see from Figure 9 that for the recent epochs, the SV power at spherical harmonic degree 10 for the dispersion in the ensemble of

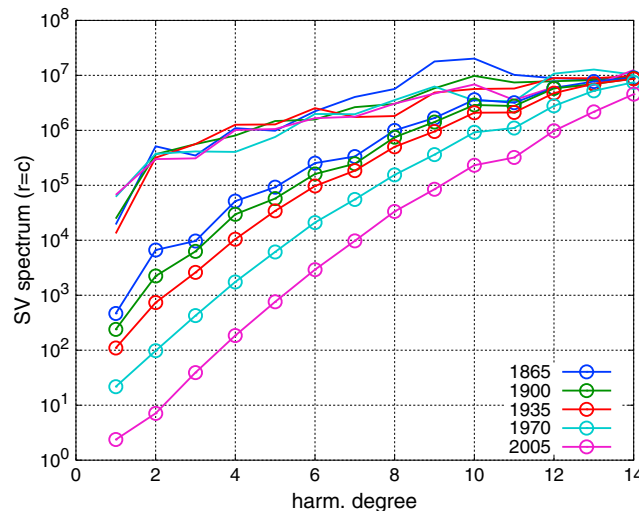


Figure 9. SV spatial power spectra $S_{SV}(n)$ (solid lines) and $S_{\delta SV}(n)$ (lines with circles) at the CMB, in $(nT/yr)^2$, as defined by equations (19) and (20), epochs between 1865 to 2005 every 35 years.

realizations is about 10% of the power for the ensemble average of realizations. This suggests about 30% errors on the SV, compared to about 100% errors in degree 10 coefficients before 1960. We also note from Figure 9 that the SV is completely governed by the random process at spherical harmonic degree 14, which suggests there is no need to increase N_i further in our explicit modeling of the SV.

[52] Variances do not however contain all the required information, since we find that some non-diagonal elements of the a posteriori covariance matrix are significant. The cross-covariances between SV coefficients,

$$c_{nn'}^{mm'}(t, t') = E \left[\left(\frac{\partial g_n^m}{\partial t}(t) - \frac{\partial \bar{g}_n^m}{\partial t}(t) \right) \left(\frac{\partial g_{n'}^{m'}}{\partial t}(t') - \frac{\partial \bar{g}_{n'}^{m'}}{\partial t}(t') \right) \right], \quad (21)$$

should not be ignored when building the SV errors model required for reconstructing core flows. From (21), we define the correlation between coefficients at a given epoch,

$$r_{nn'}^{mm'}(t) = c_{nn'}^{mm'}(t, t) / \sqrt{c_{nn}^{mm}(t) c_{n'n'}^{m'm'}(t)}, \quad (22)$$

which we plot in Figure 10 for epochs 1925 (lower triangular matrix, below diagonal) and 2005 (upper triangular matrix, above diagonal).

[53] We observe a particularly strong anti-correlation (larger than 0.5 in amplitude) between errors in $\partial g_n^m / \partial t$ and $\partial g_{n+1}^m / \partial t$ during the first part of the twentieth century. We attribute this correlation to the uneven distribution of magnetic observatories,

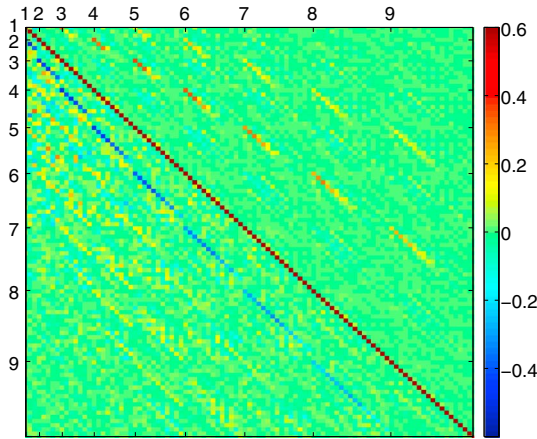


Figure 10. Correlation between the posterior errors on the COV-OBS SV coefficients, for all degrees and orders, at epochs 1925 (lower triangular matrix, below diagonal) and 2005 (upper triangular matrix, above diagonal). Spherical harmonic degrees n are indicated on the x and y axis, and coefficients are sorted as follows: $g_1^0, g_1^1, h_1^1, g_2^0, g_2^1, h_2^1, g_2^2, h_2^2, g_3^0, \dots$

which was exacerbated in the first half of the twentieth century. It decreases going back into the nineteenth century when more maritime data is available (not shown). The last point is also partly explained by the fact that with poorer quality data at earlier epochs, the error statistics tend to be dominated by the prior information, in which all degrees and orders are independent. This correlation decreases toward the most recent epochs and disappears during the satellite era. There it is replaced by a surprising positive correlation between coefficients $\partial g_n^m / \partial t$ and $\partial g_{n+2}^m / \partial t$. As only orders $m \leq 2$ are concerned, we suspect here an effect of the ambiguity between internal and large length-scale external sources from instantaneous satellite observations, which largely averages out when considering only annual means from observatories (see section 3.2). We only weakly find the negative correlations mentioned by *Ultré-Guérard et al.* [1998] between g_n^m and g_{n+2}^m coefficients for the period 1980–2000 (see their Figure 5).

4. Perspectives Arising From Stochastic Geomagnetic Field Modeling

4.1. Different Priors for Different Timescales

[54] The correlation function (see equation (13)) that we use to embody our prior knowledge about the time variation of the geomagnetic field coefficients on decadal to centennial timescales corresponds to a power spectrum $S(f) \sim |f|^{-4}$. On longer timescales, we lack detailed magnetic records of duration long compared to $\tau_g(n)$. Yet we have some knowledge of the power spectrum of paleomagnetic series [see, e.g., *Panovska, 2012, Figure 4.6*] and of the Earth's dipole moment [*Constable and Johnson, 2005*], which indicate $S(f) \sim |f|^{-2}$ in the period range $10^3 - 10^5$ years. The dipole moment power spectrum calculated from geodynamo simulations also displays power law exponents of about -2 and -4 for frequencies, respectively, below and above 400 year^{-1} [*Olson et al., 2012*].

[55] The power law f^{-4} corresponds to the asymptotic behavior, at high frequencies, of the AR(2) stochastic process that obeys equation (12), whereas the power law f^{-2} corresponds to the AR(1) stochastic process φ defined by

$$\frac{d\varphi}{dt} + \tau_c^{-1}\varphi = \varepsilon(t). \quad (23)$$

The correlation function of such a process is the Matérn function defined by (10) with $\nu = 1/2$, which is the Laplace function $\rho(\tau) = \exp(-|\tau/\tau_c|)$.

[56] The apparent continuity and differentiability properties of the observed magnetic changes depend on the sampling frequency at which they are recorded. The AR(2) process (12) used throughout our study is continuous and differentiable once, while on the other hand, the AR(1) process defined by equation (23) is continuous but not differentiable. Although the AR(2) process fits well with the observation of “jerks” on decadal timescales, the AR(1) process seems more appropriate for geomagnetic time series with a coarser resolution and appears more compatible with the observation of archeomagnetic jerks [Gallet *et al.*, 2003]. The virtual axial dipole moment series obtained from both the paleomagnetic record [Brendel *et al.*, 2007] and geodynamo simulations [Kuipers *et al.*, 2009] have also previously been interpreted as realizations of the AR(1) process (23) with $\tau_c \simeq 2.10^4$ years.

4.2. Regarding the Geomagnetic Secular Variation as a Continuous Time Autoregressive Process

[57] A further improvement to the modeling scheme adopted in the present study may in the future allow better exploitation of the information contained in geomagnetic data. By assuming a variance and an autocorrelation function $\rho(\tau)$ for the Gauss coefficients, it is in fact possible to directly obtain time sequences of field coefficients from irregularly sampled magnetic records. Such an approach can be illustrated by the following idealized scenario where input data, listed in a vector \mathbf{x} , consist of estimates of a particular field coefficient at specific times and model predictions \mathbf{f} for this coefficient are sought at desired times. The posterior mean solution to this problem can be written as

$$\bar{\mathbf{f}} = \mathbf{C}_{fx}[\mathbf{C}_{xx} + \mathbf{C}_{ee}]^{-1} \mathbf{x} \quad (24)$$

where \mathbf{C}_{xx} denotes the matrix of coefficient covariances between the times when data are available, \mathbf{C}_{fx} is the matrix of coefficient covariances between times when data are available and times when the model is evaluated, and \mathbf{C}_{ee} is the covariance matrix for the data errors [see Rasmussen and Williams, 2006, p. 17]. Interestingly, it is in principle possible within this framework to account for dating uncertainties, which constitutes a major source of errors when building geomagnetic field models for the Holocene [e.g., Korte *et al.*, 2011].

[58] Model time dependence in this context comes about from linear combinations of covariance functions, each centered on a data point. Similar approaches have been extensively studied by the

geodetic community [e.g., Moritz, 1980; Sabaka *et al.*, 2010], where this approach is known as least-squares collocation. By adopting this method for geomagnetic field modeling, one could avoid the undesirable filtering that results from projection onto B-splines (see Appendix A). In the present study, which is a first step toward a more consistent treatment based on stochastic processes, we retained the spline basis due to its well developed apparatus in the context of field modeling.

[59] The magnetic field models *COV-OBS* (mean and posterior covariance matrix) are available at <http://www.spacecenter.dk/files/magnetic-models/COV-OBS/>

Appendix A: Covariance Matrix for Spline Model Coefficients

[60] We describe here how we approximate the projection of true series $\hat{g}(t)$ onto splines of order J and knot spacing Δt (the method is given here for a single series). Given an auto-covariance function $C_{\hat{g}}(\tau)$ for the “true” core coefficient series $\hat{g}(t)$, we build the covariance matrix for a sample of observations $\mathbf{g}^o = [\hat{g}(t_1) \dots \hat{g}(t_2)]$ every $\delta t \ll \Delta t$. We denote $\mathbf{C}_{g^o} = E(\mathbf{g}^o \mathbf{g}^{oT})$ this matrix, which is of rank $K = (t_2 - t_1)/\delta t + 1$. An ensemble of samples for such “true” series can be obtained from a random variable vector with zero mean and unit variance and the Cholesky decomposition of \mathbf{C}_{g^o} (cf. end of section 2.3).

[61] The prediction vector $\mathbf{g}^p = [g(t_1) \dots g(t_2)]$ of the spline fit to \mathbf{g}^o is related to a spline model $\mathbf{g} = [g_1 \dots g_P]$ through an operator \mathbf{A} . This is built from the expression

$$g(t) = \sum_{i=1}^P B_i(t) g_i \quad (A1)$$

and depends on the knot spacing Δt and the spline order J (B_i are B-spline functions): $\mathbf{g}^p = \mathbf{A}(J, \Delta t) \mathbf{g}$. The projection onto splines is obtained by minimizing the cost function

$$\sum_{k=1}^K (g_k^o - g_k^p)^2 = [\mathbf{g}^o - \mathbf{A} \mathbf{g}]^T [\mathbf{g}^o - \mathbf{A} \mathbf{g}]. \quad (A2)$$

The best least-squares fit is then given by

$$\mathbf{g}^* = (\mathbf{A}^T \mathbf{A})^{-1} \mathbf{A}^T \mathbf{g}^o = \mathbf{H} \mathbf{g}^o, \quad (A3)$$

and the resulting covariance matrix relevant to the spline models coefficients $\{g_i\}_{i=1,P}$ is then

$$C_g = E(\mathbf{g}\mathbf{g}^T) = \mathbf{H}C_{g^e}\mathbf{H}^T. \quad (\text{A4})$$

Appendix B: Squared-exponential Gaussian Correlation Functions

[62] Let us denote by C_φ the auto-covariance function of a stationary, real-valued, continuous, and twice mean-square differentiable process $\varphi(t)$. We consider the auto-covariance of the derivative $\dot{\varphi}(t)$ and of the second time derivative $\ddot{\varphi}(t)$. We have [Hulot and Le Mouél, 1994; Stein, 1999, p. 21]

$$C_{\dot{\varphi}}(\tau) = -\frac{d^2 C_\varphi(\tau)}{d\tau^2}, \quad C_{\ddot{\varphi}}(\tau) = \frac{d^4 C_\varphi(\tau)}{d\tau^4}. \quad (\text{B1})$$

[63] We now turn to the case of squared-exponential Gaussian functions, whose correlation function is

$$\rho(\tau) = \frac{C_\varphi(\tau)}{C_\varphi(0)} = \exp\left[-\frac{1}{2}\left(\frac{\tau}{\tau_c}\right)^2\right], \quad (\text{B2})$$

where τ_c is a typical correlation time for the process. Its second and fourth derivatives are

$$\frac{d^2 \rho}{d\tau^2}(\tau) = \frac{\rho(\tau)}{\tau_c^2} \left[-1 + \left(\frac{\tau}{\tau_c}\right)^2\right], \quad (\text{B3})$$

$$\frac{d^4 \rho}{d\tau^4}(\tau) = \frac{\rho(\tau)}{\tau_c^4} \left[3 - 6\left(\frac{\tau}{\tau_c}\right)^2 + \left(\frac{\tau}{\tau_c}\right)^4\right]. \quad (\text{B4})$$

Combining equations (B1) to (B4), we deduce the variances for the first and second time derivatives of a squared-exponential process $\varphi(t)$,

$$C_{\dot{\varphi}}(0) = -C_\varphi(0) \frac{d^2 \rho}{d\tau^2}(0) = \frac{C_\varphi(0)}{\tau_c^2}, \quad (\text{B5})$$

$$C_{\ddot{\varphi}}(0) = C_\varphi(0) \frac{d^4 \rho}{d\tau^4}(0) = \frac{3C_\varphi(0)}{\tau_c^4}, \quad (\text{B6})$$

from which we obtain the analytical relation

$$C_{\ddot{\varphi}}(0) = \frac{3C_{\dot{\varphi}}^2(0)}{C_\varphi(0)}. \quad (\text{B7})$$

[64] We now apply this result to magnetic field model coefficients: $C_{\dot{g}}(n, \tau)$ and $C_{\ddot{g}}(n, \tau)$ correspond to the auto-covariance functions for the first and second time derivative of degree n coefficients. Using equation (B7) and the notations of section 2.4, we obtain the condition

$$\forall n, \quad \tau_{\dot{g}}^2(n) = \frac{1}{3}\tau_g^2(n), \quad (\text{B8})$$

which is inconsistent with the observation of rapidly changing SV at low spherical harmonic degrees (also see our interpretation of SA models in section 2.5).

[65] In addition, Stein [1999] provides further convincing arguments as to why the function (B2) is not appropriate for modeling a physical process. For instance, he remarks that knowing the corresponding process $\varphi(t)$ for $-\varepsilon \leq t \leq 0$ suffices to predict $\varphi(t)$ perfectly for $0 \leq t \leq \infty$, even if ε is small. It is not realistic to assume that knowing the Earth's magnetic field for a short time interval dramatically enhances our ability to predict the future evolution of the field.

Acknowledgments

[66] We are grateful to the referees V. Lesur and T. Sabaka for their deep reading of the manuscript and their constructive comments that helped greatly improve the quality of the paper. We thank the national institutes that support ground magnetic observatories and INTERMAGNET for promoting high standards of practice, and the institutes responsible for the CHAMP, Ørsted, and SAC-C missions for operating the satellites and making the data available. We thank the Observatoire des Sciences de l'Univers de Grenoble for financing a 1 month visit of CF in Grenoble and the International Space Science Institute for providing support for the workshops of international team no. 167. This work was supported in part by the French Centre National d'Etudes Spatiales (CNES) for the preparation of the Swarm mission of ESA. This work has been partially supported by the French Agence Nationale de la Recherche under the grant ANR-11-BS56-011.

References

- Backus, G. E. (1983), Application of mantle filter theory to the magnetic jerk of 1969, *Geophys. J. R. astr. Soc.*, *74*, 713–746.
- Backus, G. E. (1988), Bayesian inference in geomagnetism, *Geophysical Journal*, *92*, 125–142.
- Bartels, J. (1963), Discussion of time-variations of geomagnetic activity, indices Kp and Ap, 1932–1961, *Annales de Geophysique*, *19*, 1.
- Beggan, C., and K. Whaler (2009), Forecasting change of the magnetic field using core surface flows and ensemble Kalman filtering, *Geophys. Res. Lett.*, *36*(18).
- Bloxham, J., and A. Jackson (1992), Time-dependent mapping of the magnetic field at the core-mantle boundary, *J. Geophys. Res.*, *97*, 19,537–19,563.
- Bouligand, C., G. Hulot, A. Khokhlov, and G. A. Glatzmaier (2005), Statistical paleomagnetic field modeling and dynamo numerical simulation, *Geophys. J. Int.*, *161*, 603–626.
- Brendel, K., J. Kuipers, G. Barkema, and P. Hoyng (2007), An analysis of the fluctuations of the geomagnetic dipole, *Phys. Earth Planet. Inter.*, *162*, 249–255.

- Cain, J. C., and R. E. Sweeney (1973), The POGO data, *J. Atmos. Terr. Phys.*, **35**, 1231–1247.
- Christensen, U. R., I. Wardinski, and V. Lesur (2012), Timescales of geomagnetic secular acceleration in satellite field models and geodynamo models, *Geophys. J. Int.*, **190**, 243–254, doi:10.1111/j.1365-246X.2012.05508.x.
- Constable, C., and C. Johnson (2005), A paleomagnetic power spectrum, *Phys. Earth Planet. Int.*, **153**(1–3), 61–73.
- Currie, R. G. (1968), Geomagnetic spectrum of internal origin and lower mantle conductivity, *J. Geophys. Res.*, **73**, 2779–2786.
- de Boor, C. (2001), *A Practical Guide to Splines*, Springer.
- De Santis, A., D. Barraclough, and R. Tozzi (2003), Spatial and temporal spectra of the geomagnetic field and their scaling properties, *Phys. Earth Planet. Int.*, **135**(2), 125–134.
- Eymin, C., and G. Hulot (2005), On core surface flows inferred from satellite magnetic data, *Phys. Earth Planet. Inter.*, **152**, 200–220.
- Finlay, C. C., A. Jackson, N. Gillet, and N. Olsen (2012), Core surface magnetic field evolution 2000–2010, *Geophys. J. Int.*, **189**, 761–781, doi:10.1111/j.1365-246X.2012.05395.x.
- Fournier, A., J. Aubert, and E. Thébault (2011), Inference on core surface flow from observations and 3-D dynamo modelling, *Geophys. J. Int.*, **186**, 118–136.
- Gallet, Y., A. Genevey, and V. Courtillot (2003), On the possible occurrence of “archaeomagnetic jerks” in the geomagnetic field over the past three millennia, *Earth Planet. Sci. Lett.*, **214**(1–2), 237–242, doi:10.1016/S0012-821X(03)00362-5.
- Gavoret, J., D. Gibert, M. Menvielle, and J.-L. L. Mouël (1986), Long-term variations of the external and internal components of the Earth’s magnetic field, *J. Geophys. Res.*, **91**, 4787–4796.
- Gillet, N., M. A. Pais, and D. Jault (2009), Ensemble inversion of time-dependent core flow models, *Geochem. Geophys. Geosyst.*, **10** (6), Q06,004, doi:10.1029/2008GC002,290.
- Gillet, N., V. Lesur, and N. Olsen (2010), Geomagnetic core field secular variation models, *Space Sci. Rev.*, doi:10.1007/s11,214-009-9586-6.
- Gubbins, D. (1983), Geomagnetic field analysis—I. Stochastic inversion, *Geophys. J. R. Astr. Soc.*, **73**, 641–652.
- Gubbins, D., and J. Bloxham (1985), Geomagnetic field analysis—III. Magnetic fields on the core-mantle boundary, *Geophys. J. R. Astr. Soc.*, **80**, 695–713.
- Haines, G. V. (1993), Modelling geomagnetic secular variation by main-field differences, *Geophys. J. Int.*, **114**(3), 490–500, doi:10.1111/j.1365-246X.1993.tb06982.x.
- Holme, R. (2007), Large scale flow in the core, in *Treatise in Geophysics, Core Dynamics*, vol. 8, edited by P. Olson and G. Schubert, chap. 4, pp. 107–129, Elsevier.
- Holme, R., and J. Bloxham (1996), The treatment of attitude errors in satellite geomagnetic data, *Phys. Earth Planet. Inter.*, **98**, 221–223.
- Holme, R., N. Olsen, and F. Baird (2011), Mapping geomagnetic secular variation at the core-mantle boundary, *Geophys. J. Int.*, **186**, 521–528.
- Hongre, L., G. Hulot, and A. Khokhlov (1998), An analysis of the geomagnetic field over the past 2000 years, *Phys. Earth Planet. Int.*, **106**, 311–335.
- Hulot, G., and J.-L. Le Mouël (1994), A statistical approach to the Earth’s main magnetic field, *Phys. Earth Planet. Int.*, **82**, 167–183.
- Jackson, A., and C. C. Finlay (2007), Geomagnetic secular variation and applications to the core, in *Treatise in Geophysics, Geomagnetism*, vol. 5, chap. 5, pp. 147–193, eds. M. Kono and G. Schubert.
- Jackson, A., and P. Livermore (2009), On Ohmic heating in the Earth’s core I: Nutation constraints, *Geophys. J. Int.*, pp. doi: 10.1111/j.1365-246X.2008.04,008.x.
- Jackson, A., A. R. T. Jonkers, and M. R. Walker (2000), Four centuries of geomagnetic secular variation from historical records, *Phil. Trans. R. Soc. Lond. A*, **358**, 957–990.
- Jazwinski, A.H. (1970), *Stochastic Processes and Filtering Theory*, Academic Press, New York.
- Jonkers, A. R. T., A. Jackson, and A. Murray (2003), Four centuries of geomagnetic data from historical records, *Rev. Geophys.*, **41**, 1006 doi:10.1029/2002RG000,115.
- Korte, M., C. Constable, F. Donadini, and R. Holme (2011), Reconstructing the holocene geomagnetic field, *Earth Planetary Science Letters*, **312**, 497–505.
- Kuang, W., A. Tangborn, Z. Wei, and T. Sabaka (2009), Constraining a numerical geodynamo model with 100-years of geomagnetic observations, *Geophys. J. Int.*, **179**, 1458–1468.
- Kuipers, J., P. Hoyng, J. Wicht, and G. Barkema (2009), Analysis of the variability of the axial dipole moment of a numerical geodynamo model, *Phys. Earth Planet. Int.*, **173**(3–4), 228–232, doi:10.1016/j.pepi.2008.12.001.
- Kuvshinov, A., and N. Olsen (2006), A global model of mantle conductivity derived from 5 years of CHAMP, Ørsted, and SAC-C magnetic data, *Geophys. Res. Lett.*, **33**, L18301, doi:10.1029/2006GL027083.
- Langel, R. A., and R. H. Estes (1985a), The near-Earth magnetic field at 1980 determined from MAGSAT data, *J. Geophys. Res.*, **90**, 2495–2510.
- Langel, R. A., and R. H. Estes (1985b), Large-scale, near-field magnetic fields from external sources and the corresponding induced internal field, *J. Geophys. Res.*, **90**, 2487–2494.
- Langel, R. A., J. R. Ridgeway, M. Sugiura, and K. Maezawa (1988), The geomagnetic field at 1982 from DE-2 and other magnetic field data, *J. Geomag. Geoelectr.*, **40**, 1103–1127.
- Langel, R. A., T. J. Sabaka, R. T. Baldwin, and J. A. Conrad (1996), The near-Earth magnetic field from magnetospheric and quiet-day ionospheric sources and how it is modeled, *Phys. Earth Planet. Int.*, **98**, 235–267.
- Lesur, V., I. Wardinski, M. Hamoudi, and M. Rother (2010a), The second generation of the GFZ reference internal magnetic model: GRIMM-2, *Earth Planets Space*, **62**, 765–773.
- Lesur, V., I. Wardinski, S. Asari, B. Minchev, and M. Manda (2010b), Modelling the Earth’s core magnetic field under flow constraints., *Earth Planets Space*, **62**, 503–516.
- Lühr, H., and S. Maus (2010), Solar cycle dependence of quiet-time magnetospheric currents and a model of their near-Earth magnetic field, *Earth Planets Space*, **62**, 843–848.
- McLeod, M. G. (1996), Spatial and temporal power spectra of the geomagnetic field, *J. Geophys. Res.*, **101**, 2745–2763.
- Moritz, H. (1980), *Advanced Physical Geodesy*, Herbert Wichmann Verlag, Karlsruhe.
- Neubert, T., et al. (2001), Ørsted satellite captures high-precision geomagnetic field data, *Eos, Transactions American Geophysical Union*, **82**, 81.
- Olsen, N., and M. Manda (2007), Investigation of a secular variation impulse using satellite data: The 2003 geomagnetic jerk, *Earth Planetary Science Letters*, **255**, 94–105.
- Olsen, N., H. Lühr, T. J. Sabaka, and M. Manda (2006), CHAOS—A model of Earth’s magnetic field derived from CHAMP, Oersted, and SAC-C magnetic satellite data, *Geophys. J. Int.*, **166**, 67–75.
- Olsen, N., M. Manda, T. Sabaka, and L. Tøffner-Clausen (2010a), The CHAOS-3 geomagnetic field model and candidates for the 11th generation IGRF, *Earth Planets Space*, **62**, 719–727.

- Olsen, N., H. Lühr, T. Sabaka, I. Michaelis, J. Rauberg, and L. Tøffner-Clausen (2010b), CHAOS-4—A high-resolution geomagnetic field model derived from low-altitude CHAMP data, *American Geophysical Union Fall Meeting*, abstract no. GP21A-0992.
- Olson, P. L., U. R. Christensen, and P. E. Driscoll (2012), From superchrons to secular variation: A broadband dynamo frequency spectrum for the geomagnetic dipole, *Earth Planetary Science Letters*, 319–320, 75–82, doi:10.1016/j.epsl.2011.12.008.
- Pais, M. A., and D. Jault (2008), Quasi-geostrophic flows responsible for the secular variation of the Earth's magnetic field, *Geophys. J. Int.*, 173, 421–443.
- Panovska, S. (2012), Modelling holocene geomagnetic field evolution, Ph.D. Thesis, ETH (Zürich).
- Percival, D., and A. Walden (1993), Spectral Analysis for Physical Applications: Multitaper and Conventional Univariate Techniques, Cambridge University Press.
- Pinheiro, K., and A. Jackson (2008), Can a 1-D mantle electrical conductivity model generate magnetic jerk differential time delays?, *Geophys. J. Int.*, 173, 781–792.
- Rasmussen, C. E., and C. K. I. Williams (2006), Gaussian Processes for Machine Learning, The MIT Press, Cambridge.
- Reigber, C., H. Lühr, and P. Schwintzer (2002), CHAMP mission status, *Adv. Space Res.*, 30, 129–134.
- Sabaka, T., R. Langel, R. Baldwin, and J. Conrad (1997), The geomagnetic field 1900–1995, including the large-scale field from magnetospheric sources, and the NASA candidate models for the 1995 revision of the IGRF, *J. Geomag. Geoelectr.*, 49, 157–206.
- Sabaka, T. J., N. Olsen, and M. E. Purucker (2004), Extending comprehensive models of the Earth's magnetic field with Oersted and CHAMP data, *Geophys. J. Int.*, 159, 521–547.
- Sabaka, T. J., D. D. Rowland, S. B. Luthcke, and J.-P. Boy (2010), Improving global mass flux solutions from Gravity Recovery and Climate Experiment (GRACE) through forward modeling and continuous time correlation, *J. Geophys. Res.*, 115 (B11403), doi:10.1029/2010JB007533.
- Schmucker, U. (1991), Solar cycle variations and corrected annual means for external effects at Fürstfeldbruck 1951–1968, in “150 Years Earthmagnetic Observatories München - Maisach - Fürstfeldbruck”, Vol. 5, 217–248 pp., eds M. Beblo and H. Soffel, München, Münchner Geophysikalische Mitteilungen.
- Siebert, M., and J. Meyer (1996), Geomagnetic activity indices, The Upper Atmosphere: Data Analysis and Interpretation (*Eds. W. Dieminger, G.K. Hartmann, R. Leitinger*), pp. 887–911.
- Silverman, B. (1984), Spline smoothing: The equivalent variable kernel method, *Annals of Statistics*, 12, 898–916.
- Sivia, D. S., and J. Skilling (2006), Data Analysis. A Bayesian tutorial, Oxford University Press, Oxford.
- Stein, M. (1999), Interpolation of Spatial Data: Some Theory for Kriging, Springer-Verlag, New-York.
- Ultré-Guérard, P., D. Jault, M. Alexandrescu, and J. Achache (1998), Improving geomagnetic field models for the period 1980–1999 using Ørsted data, *Earth Planets Space*, 50, 635–640.
- Velínský, J. (2010), Electrical conductivity in the lower mantle: Constraints from champ satellite data by time-domain EM induction modelling, *Phys. Earth Planet. Int.*, 180 (3–4), 111–117, doi:10.1016/j.pepi.2010.02.007.
- Velínský, J., and C. C. Finlay (2011), Effect of a metallic core on transient geomagnetic induction, *Gechem. Geophys. Geosyst.*, 12 (5), Q05,011, doi:10.1029/2011GC003557.
- Von Kármán, T. (1948), Progress in the statistical theory of turbulence, *Proc. Natl. Acad. Sci. USA*, 34(11), 530–539.
- Wardinski, I., and R. Holme (2011), Signal from noise in geomagnetic field modelling: Denoising data for secular variation studies, *Geophys. J. Int.*, 185, 653–662.
- Wardinski, I., and V. Lesur (2012), An extended version of the C³FM geomagnetic field model—Application of a continuous frozen-flux constraint, *Geophys. J. Int.*, 189, 1409–1429, doi:10.1111/j.1365-246X.2012.05384.x..
- Yaglom, A. (1987), Correlation Theory of Stationary and Related Random Functions, Springer-Verlag, New York.
- Yukatake, T., and J. C. Cain (1979), Solar cycle variations of the first-degree spherical harmonic components of the geomagnetic field, *J. Geomag. Geoelec.*, 31, 509–544.
- Yukatake, T., and J. C. Cain (1987), Solar cycle variations in the annual mean values of the geomagnetic components of observatory data, *J. Geomag. Geoelec.*, 39, 10–49.